

A flexural-cantilever simple-shear/pure-shear model of continental lithosphere extension: applications to the Jeanne d'Arc Basin, Grand Banks and Viking Graben, North Sea

N. J. KUSZNIR¹, G. MARSDEN¹ & S. S. EGAN²

¹*Department of Earth Sciences, University of Liverpool, Liverpool,
L69 3BX, UK*

²*Department of Geology, University of Keele, Keele,
Staffs, ST5 5BG, UK*

Abstract: Mathematical models have been constructed of the geometric, thermal and flexural-isostatic response of the lithosphere to extension by faulting (simple-shear) in the upper crust and plastic, distributed deformation (pure-shear) in the lower crust and mantle. Models involving upper-crustal extension by both listric and planar faults have been developed. These coupled simple-shear/pure-shear models have been used to calculate extensional sedimentary basin geometry, subsidence history and crustal structure. Basin geometry and subsidence history are controlled by fault geometry (planar or listric), the amount of fault extension, fault dip, the depth of the transition from simple-shear to pure-shear, and the flexural rigidity of the lithosphere during both syn-rift and post-rift stages of basin formation.

For the planar fault model, footwall and hangingwall blocks are considered to behave as two interacting flexural cantilevers; the response of these cantilevers to the isostatic forces produced by extension generating footwall uplift and hangingwall collapse. For a set of adjacent planar faults the lateral superposition of flexural footwall uplift and hangingwall collapse generates the familiar 'domino'-style block-rotation of such multiple fault systems. The listric fault model assumes that the hangingwall collapses onto a rigid footwall by vertical shear, and that the tectonic denudation of the upper crust by faulting generates isostatic uplift producing limited footwall uplift. Deep seismic reflection data and earthquake seismology suggest that the fundamental basement faults controlling lithosphere extension are planar. It is argued that the vertical shear construction of hangingwall collapse onto a rigid footwall is inappropriate for basement response.

The coupled simple-shear/pure-shear models of extensional basin formation, using both listric and planar fault geometries, have been applied to the formation of the Jeanne d'Arc basin, Grand Banks, and the Viking Graben of the northern North Sea. The numerical modelling shows that the crustal thinning, thermal and sediment-fill loads generated during and after lithosphere extension need to be distributed flexurally in order to generate the observed basin depth and geometry. The flexural-cantilever, planar-fault model provides closer agreement to observed basin depth and subsidence than the listric-fault model. The planar fault model also produces more footwall uplift than a listric fault model. Erosion of this footwall uplift generates substantial isostatic uplift through unloading, leading to a large underestimate of the horizontal displacement on basin-bounding faults.

The low values of effective elastic thickness obtained by extensional basin modelling are substantially less than the thickness of the cool, brittle upper crust. It is suggested that flexural bending stresses associated with lithosphere extension on planar faults are sufficiently large to generate brittle failure within the upper crust, so producing the low values of effective elastic thickness. This is consistent with the predictions of the flexural-cantilever model.

Deep seismic reflection data show the fundamental importance of major basement faults in controlling continental lithosphere extension and the formation of major extensional sedimentary basins (Fig. 1). These major basement faults extend down into the lower crust where faulting gives way to distributed, plastic deforma-

mation. To date no unequivocal example of a major dip-slip fault or shear zone passing continuously from the surface down into the upper mantle, as suggested by the model proposed by Wernicke (1985), has been observed on any deep seismic section (Kusznir & Matthews 1988).

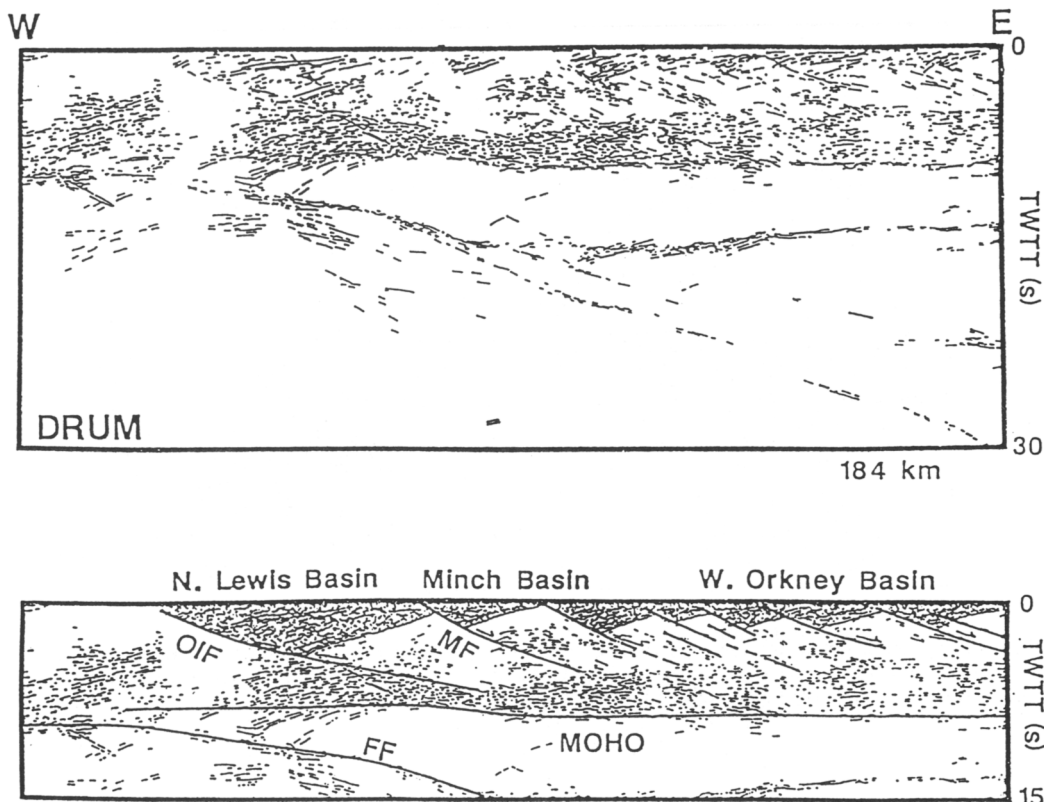


Fig. 1. Line interpretation of the DRUM deep seismic reflection profile, acquired by BIRPS to the north of Scotland, showing the control of major basement faults on lithosphere extension and sedimentary basin formation.

The major basement faults imaged on deep seismic data appear to be restricted to the cool, brittle, topmost part of the lithosphere corresponding to the seismogenic layer. Beneath the seismogenic layer, which typically has a thickness between 10 and 15 km, deformation takes place by a plastic rather than by a brittle mechanism (Jackson & McKenzie 1983; Kusznir & Park 1987). Within this region of plastic deformation in the lower crust and mantle, lithosphere extension is probably achieved by pure-shear (i.e. distributed stretching e.g. McKenzie 1978), rather than by the simple-shear (i.e. faulting) of the upper lithosphere.

Considerable debate has taken place as to whether the basement faults controlling extensional deformation within the upper and middle crust are listric or planar. Earthquake seismology (Jackson 1987) and deep seismic reflection data (e.g. Fig. 1) suggest that these fundamental basement faults are planar. However, listric faults are used by many workers in examining continental extension, probably due

to the ease with which hangingwall collapse may be computed using the vertical shear construction (Verrall 1981) or one of its many derivatives.

Lithosphere extension causes crustal thinning and perturbations of the lithosphere temperature field. Crustal thinning and lithosphere temperature field modification lead to changes in the lithosphere density field which in turn, through isostasy, generate the subsidence responsible for extensional sedimentary basin formation (McKenzie 1978 and derivatives). Both simple-shear extensional deformation in the upper crust and pure-shear deformation in the lower-crust and mantle contribute to crustal thinning and geotherm perturbation.

A quantitative model of continental extension and sedimentary basin formation should include both simple shear and pure-shear lithosphere deformation processes and their geometric, thermal and flexural-isostatic responses. Such a quantitative model would need to compute:

- (i) crustal thinning during lithosphere exten-

A FLEXURAL-CANTILEVER MODEL

43

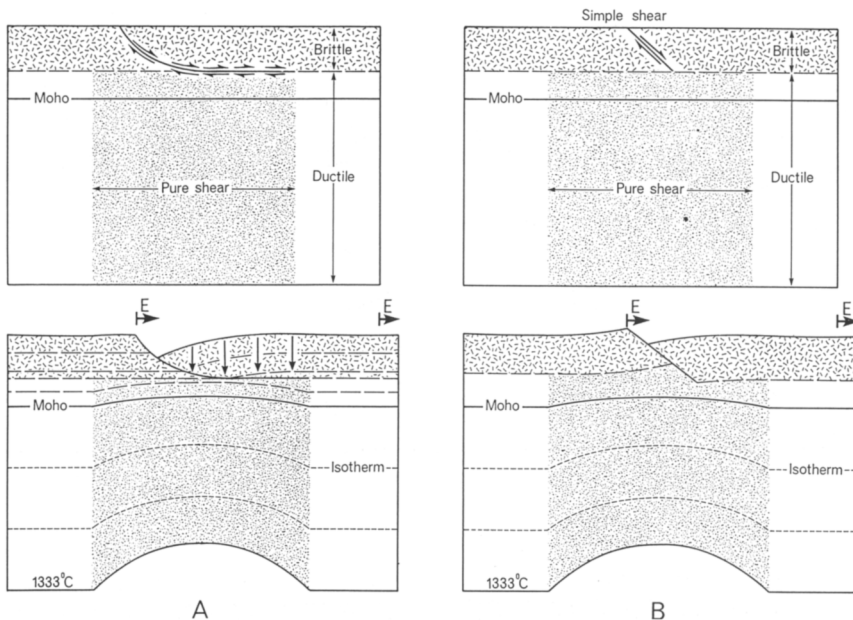


Fig. 2. A schematic representation of lithosphere extension by faulting (simple-shear) in the upper crust and pure-shear in the lower crust and mantle, showing crustal thinning and temperature field perturbation by both simple and pure-shear. (a) listric fault, (b) planar fault.

sion due to simple-shear by basement faulting in the upper crust and pure-shear (distributed plastic deformation) in the lower crust and mantle;

- (ii) perturbation of the lithosphere temperature field by both simple- and pure-shear during extension;
- (iii) thermal re-equilibration of the lithosphere temperature field after extension;
- (iv) flexural-isostatic response of the lithosphere to crustal thinning and thermal loads; both syn-rift and post-rift.

A schematic representation of lithosphere extension by simple-shear in the upper crust and pure-shear in the lower crust and mantle for both listric and planar basement fault geometries is shown in Fig. 2. A fundamental assumption of a coupled simple-shear/pure-shear model of lithosphere deformation is that upper crustal extension by faulting is balanced at depth by pure-shear stretching within the lower crust and mantle.

In the following sections of this paper, quantitative, coupled simple-shear/pure-shear models of continental lithosphere extension and basin formation, using both planar and listric faults, are presented, their fundamental properties examined, and their predictions tested.

Lithosphere extension and sedimentary basin formation on listric faults

Introduction to the model

The formulation of the model for listric faults has been described in detail elsewhere (Kusznir & Egan 1990). The listric faults are given an exponential geometry and hangingwall deformation prior to isostatic readjustment is assumed to be accomplished by vertical-shear collapse onto the footwall (Verrall 1981; Gibbs 1984). Crustal structure and basin geometry are shown in Fig. 3a at 100 Ma following lithosphere extension by 30 km on a single fault, for a listric fault detaching at 20 km depth within the lower crust. The region of pure-shear has been given a sinusoidal distribution over a width of 100 km and is situated under the listric fault. The flexural rigidity used to distribute isostatically the lithosphere loads arising from extension corresponds to an effective elastic plate thickness of 5 km. The sedimentary basin consists of a syn-rift component locally controlled by the hangingwall collapse on the listric fault, overlain by a flexurally-distributed, post-rift, thermal-subsidence component. The footwall, proximal

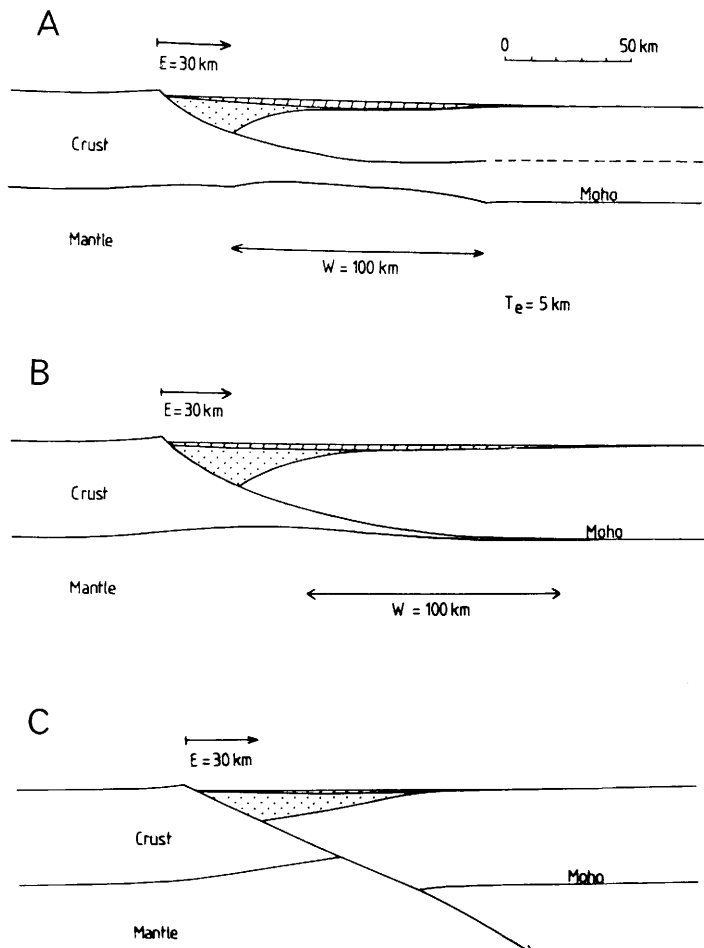


Fig. 3. Sedimentary basin geometry and crustal structure predicted by the listric fault coupled simple-shear/pure-shear model at 100 Ma after 30 km extension. Flexural rigidity corresponds to $T_e = 5$ km. W denotes the width of the pure-shear deformation. Syn-rift basin fill — dotted ornament, post-rift fill — diagonal ornament. (a) intracrustal detachment, (b) base crustal detachment, (c) base lithosphere detachment (Wernicke model).

to the footwall basement cutoff, shows uplift. This uplift is generated by the isostatic rebound of the basin region as faulting tectonically denudes the footwall, and basement material in the hanging wall of the fault is replaced by lighter sediment.

The mathematical model allows the detachment depth, the transition from brittle to ductile deformation, to be placed at any depth within the lithosphere. The McKenzie (1978) stretching model (detachment at the surface) and the Wernicke (1985) model (detachment at the base of the lithosphere) represent end members of the coupled simple-shear/pure-shear model.

Other notional variants on the model have been described by Weissel & Karner (1989). In Fig. 3b & 3c crustal structure and basin geometry are shown for a listric fault detaching at the base of the crust and the base of the lithosphere respectively. Fig. 3c represents a mathematical equivalent to the Wernicke model; however as discussed earlier no unequivocal evidence from deep seismic data exists showing faults extending continuously from the surface down to the base of the lithosphere or displacing the Moho. Application of the listric fault model to extension on multiple faults has been described in Kusznir & Egan (1990).

Application of the listric fault model to the Jeanne d'Arc Basin

The coupled simple-shear/pure-shear model of extensional sedimentary basin formation has been applied to the formation of the Jeanne d'Arc basin, Grand Banks, offshore eastern Canada (Fig. 4a). The Jeanne d'Arc basin formed by rifting beginning in the Triassic and continuing through into the early Cretaceous. The basin has been imaged by deep seismic reflection profiles (Fig. 4b) and contains a maximum sediment thickness of the order of 20 km (Keen *et al.* 1987). Tankard *et al.* (1990) on the basis of industry seismic, deep seismic and well data have constructed four regional cross sections across the Jeanne d'Arc basin, of which the two most northerly are shown in Fig. 5. The cross sections show a maximum thickness of Mesozoic basin fill of 17 km on the most northern line.

Fault positions and fault heaves for the major faults controlling the formation of the basin have been taken from the cross section shown in Fig. 5 and used to define a listric-fault, coupled simple-shear/pure-shear model of the Jeanne d'Arc basin. A simple model of the most northerly line of Fig. 5 uses two eastward-dipping faults, with fault heaves of 5.5 and 6.5 km respectively. The faults within the model are given surface dips of 60°, and the crust an initial thickness of 35 km. An average basin sediment-fill density of 2.6 g cm⁻³ has been used and is appropriate to the observed depth of the basin allowing for compaction.

Crustal structure and basin geometry using these faults positions and heaves and a detachment depth of 26 km (Tankard *et al.* 1990) are shown in Fig. 6a, predicted by the listric fault model using Airy isostasy ($T_e = 0$). The maximum depth of the basin 150 Ma after the end of rifting is 8.5 km, compared with the observed thickness of c. 17 km. Both fault geometry and Moho are highly distorted as a consequence of the local (Airy) isostasy.

The effect of using a finite flexural strength for the lithosphere ($T_e = 5$ km) is shown in Fig. 6b. The effect of flexurally distributing the isostatic forces is to deepen the basin to c. 11.5 km maximum depth. The finite flexural rigidity also leaves the Moho and fault geometries smoother and less deformed. The calculated basin depth is still substantially less than the observed 17 km. The effect of deepening the detachment depth to the base of the crust (Fig. 6c) changes the crustal structure and basin geometry and increases the footwall uplift. Deepening the detachment level does not,

however, perceptibly increase the depth of the basin.

The listric fault model does not seem able to generate the profile of Tankard *et al.* across the Jeanne d'Arc basin.

Listric versus planar faults and the inapplicability of the vertical-shear construction to basement deformation

The listric fault model does not seem able to simulate the formation of the Jeanne d'Arc basin. One possible reason may be that the major basement faults are not in reality listric. Even on time sections the major basement reflections seen on deep seismic sections (Figs 1 & 7a) appear to be straight rather than listric as they descend from the surface down into the lower crust, where they are lost in the sub-horizontal reflections of the lower crust. When depth-converted these faults are shown to be planar (Fig. 7b). This planar geometry revealed by seismic reflection data for basement extensional faults is also supported by the evidence of earthquake seismology (Jackson 1987; Stein & Barrientos 1985). Peddy (pers. comm) has shown that the major basin-bounding fault of the Jeanne d'Arc basin (Fig. 4b) is also planar when depth converted. The fundamental architecture of continental lithosphere extension, consisting of planar faults cutting the seismogenic brittle upper crust with distributed plastic deformation in the lower crust and mantle, is summarized in Fig. 2b.

If a planar basement-fault geometry is used with the hangingwall vertical-shear construction (Verrall 1981) then the crustal structure and basin geometry shown in Fig. 8 result. The basin so produced is unrealistic with a flat bottom, and inclined straight sides, and does not resemble real extensional sedimentary basins. The explanation for this unrealistic basin geometry rests with the vertical-shear construction. The vertical-shear construction assumes that the weak hangingwall collapses onto a rigid footwall, i.e. it assumes that the hangingwall is infinitely weak while the footwall is infinitely strong. This fundamental assumption of the vertical shear construction is clearly invalid for basement response, where rocks of similar rheology are juxtaposed by faulting. The vertical-shear construction is equally invalid for basement response irrespective of whether the basement faulting is planar or listric. A superior model for footwall and hangingwall lithosphere behaviour during extension would give both footwall and hangingwall blocks similar mechanical properties.

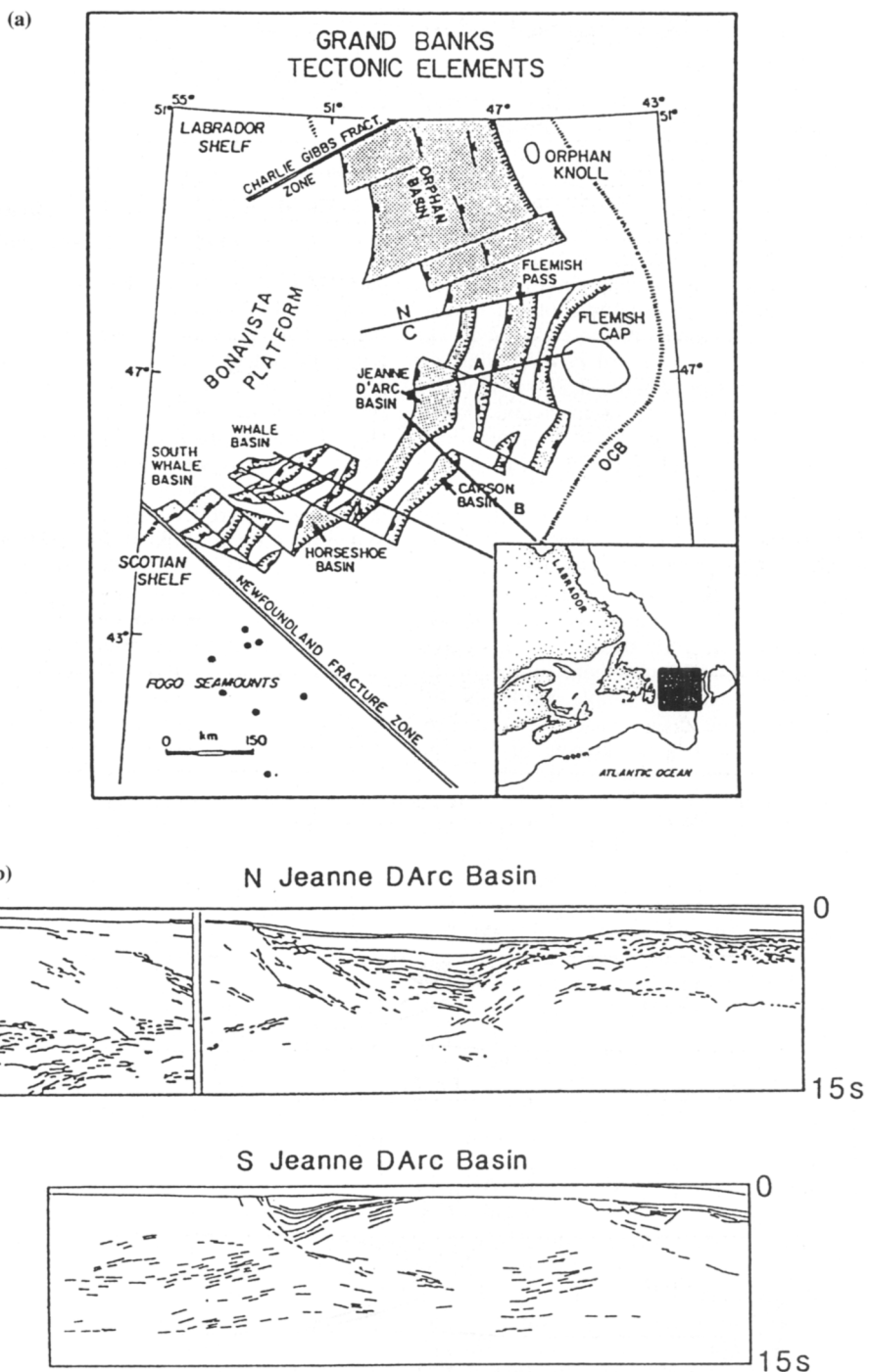


Fig. 4. (a) Location map showing the Mesozoic Jeanne d'Arc basin on the Grand Banks east of Newfoundland (Tankard *et al.* 1990). (b) Deep seismic reflection profiles (Keen *et al.* 1987) across the northern and southern Jeanne d'Arc basin.

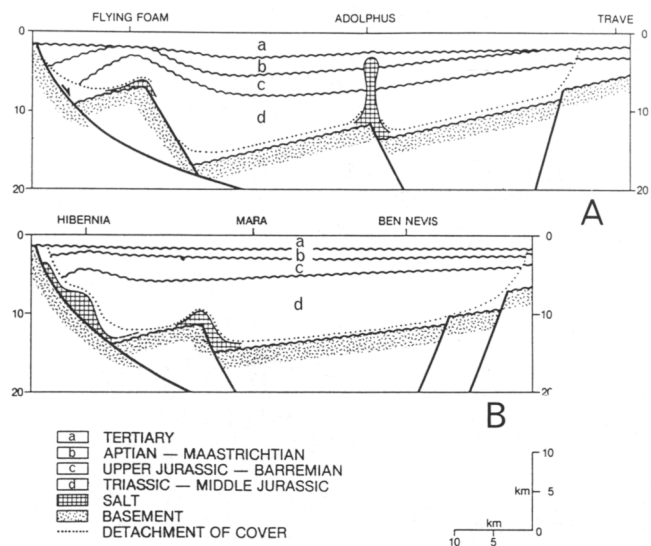


Fig. 5. Cross sections across the northern Jeanne d'Arc basin (Tankard *et al.* 1990). (a) Flying Foam — Trave profile. (b) Hibernia — Ben Nevis profile.

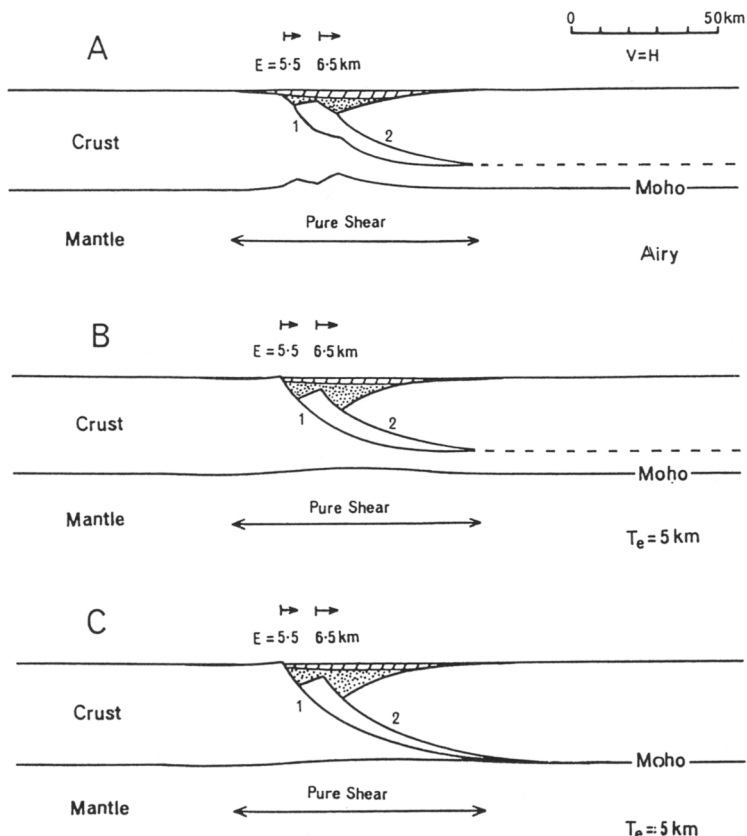


Fig. 6. Application of the listric simple-shear/pure-shear model to the Flying Foam — Trave profile across the northern Jeanne d'Arc basin (Fig. 5). Extension on fault 1 is 5.5 km and fault 2 is 6.5 km. Initial fault dip = 60°. Crustal thickness = 35 km. (a) Airy isostasy ($T_e = 0$) and detachment depth = 26 km. (b) Flexural isostasy ($T_e = 5 \text{ km}$) and detachment depth = 26 km. (c) Flexural isostasy ($T_e = 5 \text{ km}$) and detachment depth = 35 km.

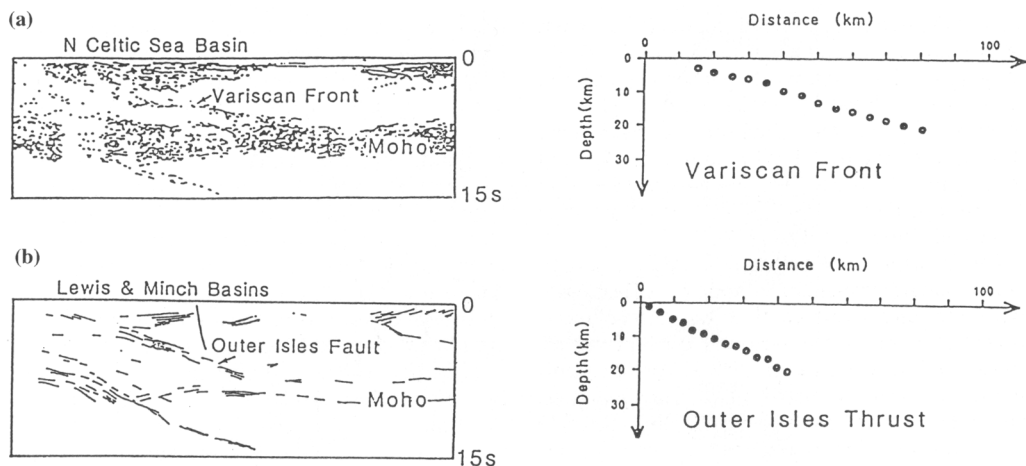


Fig. 7. (a) Deep seismic reflection profiles acquired by BIRPS across the North Celtic Sea and Lewis/Minch basin showing major extensional basement faults controlling basin formation extending down from surface to the top of the reflective lower crust at approximately 6 sec two-way traveltimes. These faults look planar rather than listric even on the time sections. (b) Depth converted fault geometries of (a) using stacking velocities, showing the planar basement faults of (a) extending down to 20 km depth.

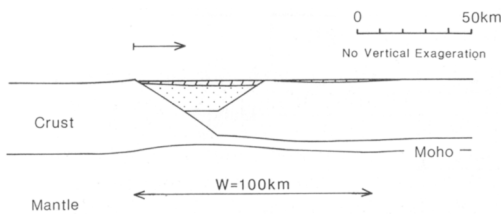


Fig. 8. An unrealistic, symmetric and flat-bottomed basin produced by extension on a planar fault using the vertical-shear hangingwall-collapse construction.

Lithosphere extension and sedimentary basin formation on planar faults

The flexural cantilever model

To overcome the problem of the vertical-shear construction when used with planar faults, a mathematical model has been developed which assumes that during extensional faulting the footwall and hangingwall blocks behave as two interacting flexural cantilevers, the response of these cantilevers to the isostatic forces produced by extension generating footwall uplift and hangingwall collapse. The hangingwall collapse so produced is generated by flexural isostatic bending of the lithosphere, as is the footwall uplift (Fig. 2b). In reality such bending may be accomplished by the summation of co-seismic

displacement during individual earthquakes and isostatic post-seismic uplift (King *et al.* 1988; Stein *et al.* 1988). This new model has been named the flexural cantilever model (Kusznir & Egan 1990).

The flexural cantilever model considers the long-term, post-seismic isostatic balance of the lithosphere following extension and is applicable over timescales $> 0.1\text{--}1.0$ Ma. It is not a dynamic, fault-growth model (cf. Walsh & Wattesson 1987) to be used over the co-seismic timescale. Co-seismically footwall and hangingwall vertical displacements during active faulting have been shown to be consistent with an elastic-dislocation process within a self-gravitating lithosphere (King *et al.* 1988). Co-seismically the flexural-isostatic process experiences a large effective elastic thickness comparable with the thickness of the lithosphere. However, as creep within the lower crust and mantle progresses with time and the initial elastic dislocation and lower lithosphere bending stresses are relieved, the effective elastic thickness of the lithosphere is greatly reduced, such that the flexural strength of the lithosphere arises solely from the brittle/elastic upper crust. Rheological modelling suggests that this post-seismic flexural-isostatic relaxation takes of the order of 0.1–1.0 Ma to reach equilibrium (Kusznir & Park 1984; Kusznir & Karner 1985). During post-seismic relaxation, footwall and hangingwall blocks are assumed to be welded together, with the lithosphere behaving as a single plate. In this

respect the flexural cantilever model differs from earlier analyses of the mechanics of footwall/hangingwall interaction during crustal extension on a planar fault by Heiskanen & Vening-Meinesz (1958) and Jackson & McKenzie (1983), who assumed that the fault is not welded as long-term isostatic balance is achieved. The flexural cantilever model is more similar to the model described by Buck (1988).

The flexural cantilever model is also a coupled simple-shear/pure-shear model of continental extension and assumes that the brittle (seismogenic) upper crust deforms by faulting on planar faults, while the ductile lower crust and mantle deform by distributed pure-shear. As with the listric fault model, the flexural cantilever model incorporates the isostatic consequences of syn-rift lithosphere temperature field perturbation and post-rift re-equilibration on sedimentary basin formation. Sediment loading effects are also included. The assumptions and behaviour of the model are summarized in Fig. 2b. The model and its mathematical formulation are described briefly in Appendix 1, and will be described in greater detail in a subsequent paper.

The calculated predictions of the flexural cantilever model are shown in Fig. 9 for lithosphere extension by 10 km on a planar fault. Crustal structure and basin geometry are shown at the end of rifting but before geotherm re-equilibration and thermal subsidence. The isostatic-loading consequences of filling the rift to a regional datum (sea level) with sediment are included. The hangingwall shows the familiar rollover geometry. The pure-shear within the lower crust and mantle is distributed symmetrically beneath the fault.

The effect of extending the lithosphere on a set of planar faults is shown in Fig. 10. For a set of adjacent planar faults the lateral superposition of flexural footwall uplift and hangingwall

collapse produces the familiar ‘domino’-style block rotation of such multiple fault systems. For each internal block, the block is flexed upward by its hangingwall fault and downward by its footwall fault, such that it is first bent one way and then unbent the other, thereby suffering a net rotation. The fault itself is also rotated, becoming shallower in dip. The region of ‘domino’-style extension terminates by footwall uplift and hangingwall collapse on its bounding faults. The flexural cantilever model also allows for multiple fault extension on unequally spaced faults with differing fault heaves and dips.

The effect of thermal subsidence on the multiple planar-fault model is shown in Fig. 10b. At the time of rifting footwall uplift can elevate fault block crests above sea level where they may be eroded. If this erosion takes place at the time of rifting, thermal re-equilibration and cooling generates a basin consisting of discrete rift sub-basins with a continuous cover of post-rift, thermal-subsidence sediment (Fig. 10c).

Application of the planar fault model to the Jeanne d'Arc Basin

Application of the flexural cantilever (planar fault) model to the Jeanne d'Arc basin is shown in Fig. 11. Similar fault position, fault heave, effective elastic thickness and other lithosphere parameters are used as in the listric model of Fig. 8. The effect of using the flexural cantilever model rather than the listric model is to deepen the basin to 14.5 km.

The planar fault model also produces more footwall uplift, approximately 2.5 km adjacent to the western basin-bounding fault given the fault heaves of Fig. 11. Today no footwall uplift is observed in this region (the Bonavista platform) and presumably any footwall uplift that had existed has now been eroded. Since the extension that gave rise to the Jeanne d'Arc basin spanned the Triassic through to Early Cretaceous, the erosion may have kept pace with footwall uplift such that the erosion may have been complete before the start of thermal subsidence in the mid Cretaceous. If erosion of the footwall uplift adjacent to the western basin-bounding fault has occurred, as it almost certainly has, then the fault heave of the basin-bounding fault seen on the section of Tankard *et al.* (1990; and Fig. 5 of this paper) and used in the models of Figs 6 and 11 must be an underestimate. Roberts & Yielding (this volume) reached similar deductions about eroded basin margins in the North Sea.

The preferred model for the northern line of

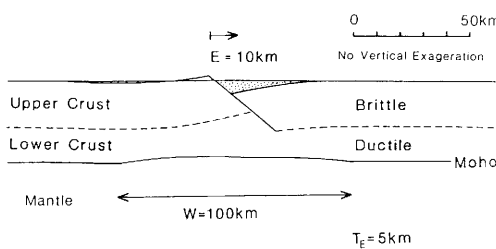


Fig. 9. Syn-rift basin geometry and crustal structure predicted by the flexural cantilever model following lithosphere extension by 10 km on a planar fault. $T_c = 5$ km. Thermal uplift and sediment loading is included in the model.

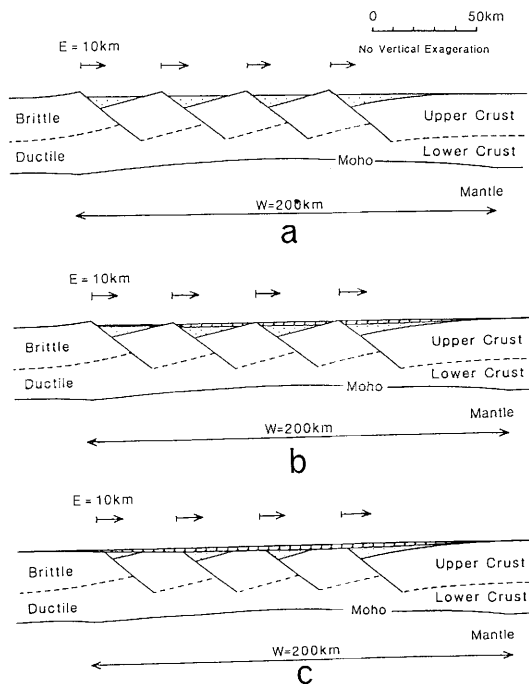


Fig. 10. Sedimentary basin geometry and crustal structure following lithosphere extension by 10 km each on 4 planar faults. (a) Syn-rift. (b) Post-rift at 100 Ma after extension. (c) Post-rift at 100 Ma after syn-rift erosion of uplifted fault block crests. Syn-rift basin-fill represented by dotted ornament and post-rift fill by diagonal ornament.

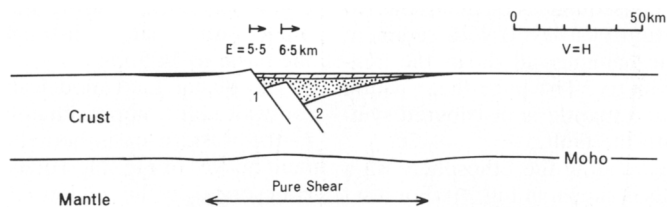


Fig. 11. Application of the flexural cantilever, planar fault model to the Flying Foam-Trave Jeanne d'Arc basin profile (Fig. 5). Extension on fault 1 is 5.5 km and fault 2 is 6.5 km. Initial fault dip = 60°. Crustal thickness = 35 km. T_e = 5 km. The planar fault model produces a deeper, broader basin than the listric model, with more footwall uplift (Fig. 6).

Tankard *et al.* across the Jeanne d'Arc is shown in Fig. 12 and has a total pre-erosion fault heave of 12 km on the basin-bounding fault. Two smaller faults (one synthetic and one antithetic) have been included in the planar fault model. The effective elastic thickness of the preferred model is 10 km. The syn-rift stage of the model is shown in Fig. 12a and shows a basin-bounding footwall uplift of c. 3 km. Erosion of this footwall uplift and the subsequent isostatic rebound, which in turn results in further erosion and

rebound, has been computed and is shown in Fig. 12b. The post-erosion heave is 5.5 km and is consistent with that observed today (Fig. 5). Some 5 km of footwall must have been eroded off the Bonavista platform basin-bounding footwall. If this erosion was distributed through the 80 Ma or so during which extension took place (Triassic to Early Cretaceous), the erosion rates of 0.07 mm a^{-1} are not unreasonable.

If the model is allowed to cool and thermally subside to a time equivalent to the present day,

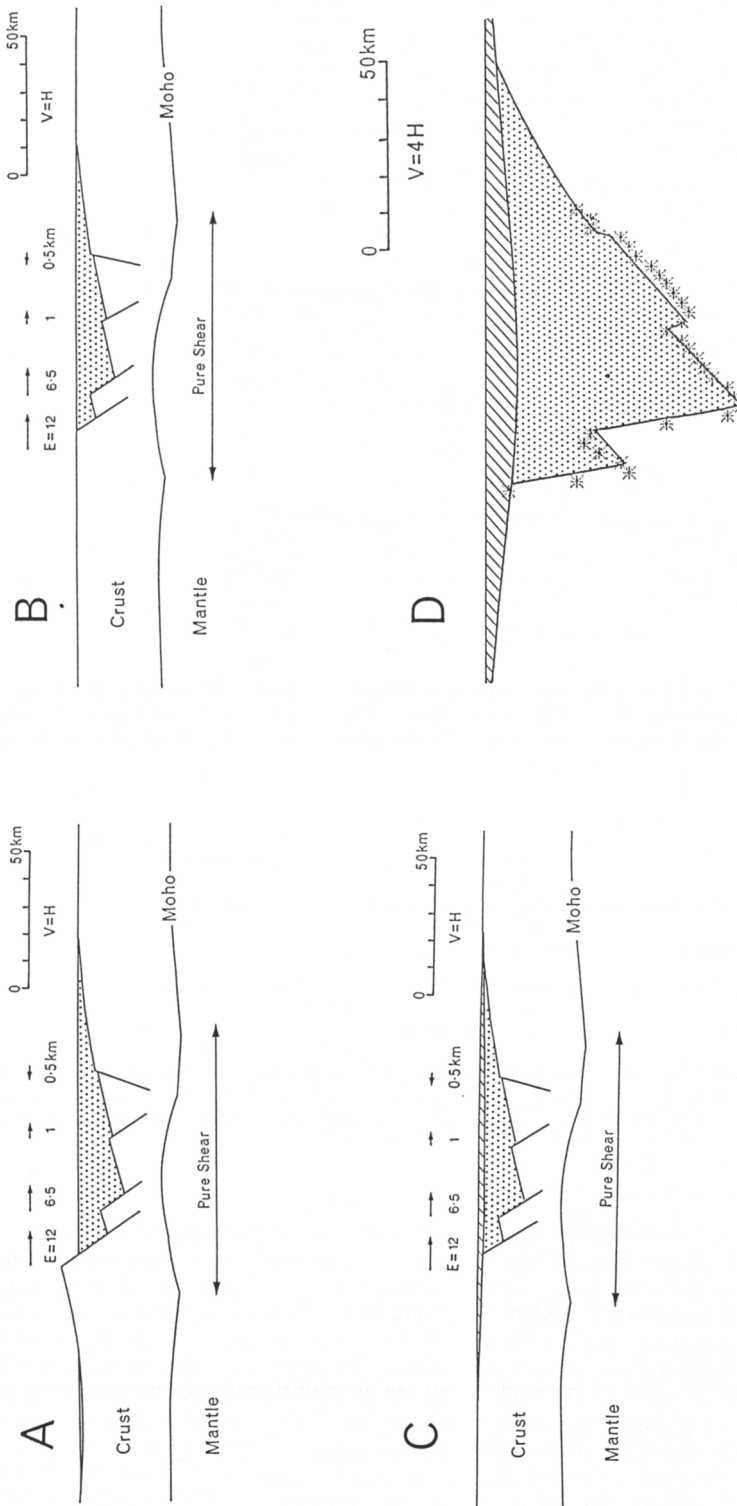


Fig. 12. The preferred flexural cantilever model of the Flying Foam – Trave profile across the Jeanne d'Arc basin. The basin-bounding fault has an extension of 12 km. The other large fault has a heave of 6.5 km. Two smaller faults have been included with fault heaves of 1 and 0.5 km – one of the faults being antithetic. Crustal thickness = 35 km, $T_e = 10$ km, and initial fault dip = 60° . (a) Basin geometry and crustal structure at syn-rift stage. (b) End syn-rift removal of footwall uplift by erosion, which has induced further flexural-isostatic rebound. (c) Present-day post-rift geometry and crustal structure. The modelled basin depth of 17 km is comparable with that observed. (d) Comparison of basin depth predicted by the flexural cantilever model (solid lines) with observed basin depth (*ornament). Vertical exaggeration = 4.

then the crustal structure and basin geometry shown in Fig. 12c results. The maximum basin depth of 17 km agrees with that observed. In Fig. 12d the observed and modelled basin depths are compared. The agreement is generally good both within the basin and on the basin flanks.

The results of modelling the second more southerly cross section of Tankard *et al.* (1990, Fig. 5) are shown in Fig. 13 for syn-rift, post-erosion, and post-rift thermal subsidence (present day) stages. The agreement between observed and model predictions are good. The flexural cantilever model gives a reasonable prediction of the observed thicknesses of syn- and post-rift sequence within the Jeanne d'Arc basin (Fig. 5).

Both the flexural cantilever and listric fault models described above are instantaneous stretching models. As discussed earlier the formation of the Jeanne d'Arc basin started in the Triassic and continued through into the Early Cretaceous, spanning a period of 80 Ma, a significantly long time compared with the thermal time-constant of the lithosphere. Compared with the instantaneous rifting model, the cooling during extension of a protracted rift model would generate more syn-rift subsidence and a higher ratio of syn- to post-rift sediments. The duration of rifting should not, however, have a major effect on the total basin depth at large times after the cessation of rifting.

The above models of the formation of the Jeanne d'Arc basin are also a simplification in that the extension direction for the Jeanne d'Arc basin changed by 90° from NW–SE during the Triassic to SW–NE during the Cretaceous (Hubbard 1988). Only extension within the plane of the sections of Tankard *et al.* (Fig. 5) has been modelled.

Discussion and conclusions

Coupled simple-shear/pure-shear models incorporating the geometric, thermal and flexural-isostatic consequences of lithosphere extension have been developed and applied to the formation of extensional sedimentary basins. The numerical modelling of the Jeanne d'Arc basin shows that the crustal thinning, thermal perturbation and sediment-fill loads generated during and after lithosphere extension need to be distributed flexurally in order to generate the observed basin depths, subsidence history and Moho topography of the Jeanne d'Arc basin.

Deep seismic reflection profiling and earthquake seismology suggest that the major faults controlling lithosphere extension are planar rather than listric. Lithosphere extension is

achieved by extension on these planar faults within the brittle upper crust and by distributed plastic stretching (pure-shear) within the lower crust and mantle. The vertical shear construction is inappropriate for modelling lithosphere extension on planar faults. Instead a model in which both footwall and hangingwall basement blocks are regarded as acting as two mutually-self-supporting flexural cantilevers is preferred. This model, the flexural cantilever model, may be applied to lithosphere extension on multiple faults and predicts the familiar 'domino-style' block rotations of extensional tectonics. In contrast to earlier multiple-fault-block rotation models (Jackson & McKenzie 1983; Barr 1987) the flexural cantilever model may be applied to faults of arbitrary spacing, horizontal displacement and throw direction, and does not require the structure to be repeated laterally to infinity.

The flexural cantilever planar fault model, when applied to the Jeanne d'Arc basin, provides closer agreement to observed basin depth and subsidence than does the listric fault model using vertical shear. The application of the flexural cantilever model to the Jeanne d'Arc basin suggests that lithosphere extension on planar basement faults generates substantial footwall uplift, leading to significant footwall erosion.

The flexural-cantilever coupled simple-shear/pure-shear model shows that the fundamental building-block of extensional sedimentary basin formation is a localized rift sub-basin overlain by a broader and thinner post-rift thermal-subsidence sub-basin (Figs 12 & 13). Extensional sedimentary basins, formed by lithosphere extension on many major faults, are generated by the superposition of the above fundamental building blocks forming a series of discrete rift sub-basins overlain by a continuous post-rift thermal subsidence basin (Fig. 10c). Because of this superposition effect multiple fault basins have a relatively thicker post-rift thermal subsidence sequence than single fault basins.

The Viking Graben, North Sea

This effect can be illustrated by the application of the flexural cantilever model to the formation of the Viking Graben, northern North Sea (Marsden *et al.* 1990). Both Triassic and Jurassic stages of rifting have been modelled, and compaction is included. Jurassic fault extensions and positions, for input to the mathematical model, have been determined using industry seismic reflection data (Figure 2 of Marsden *et al.* 1990). Crustal structure, basin geometry and the thicknesses of syn- and post-rift se-

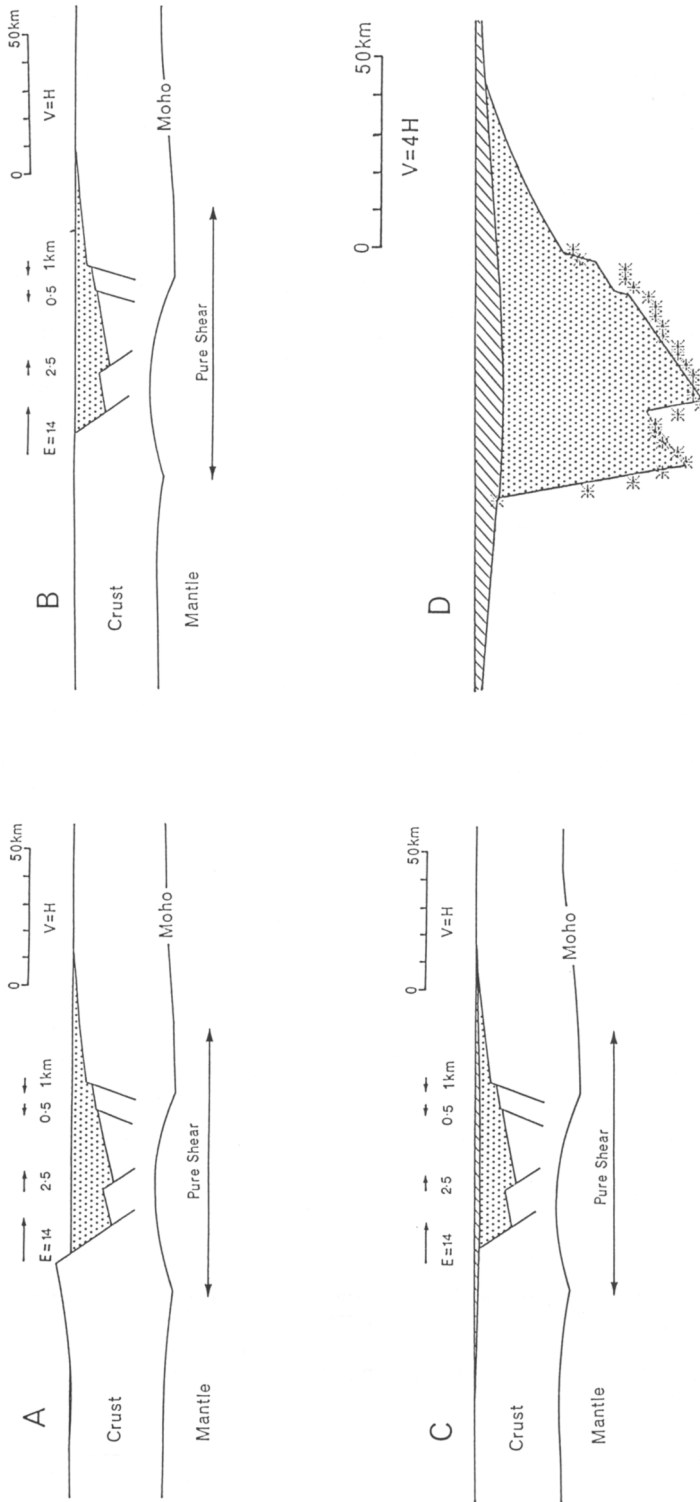


Fig. 13. The preferred flexural cantilever model of the Hibernia – Ben Nevis profile across the Jeanne d'Arc basin. The basin-bounding fault has an extension of 14 km. Three smaller faults have fault heaves of 2.5, 0.5 and 0.5 km – two of these smaller faults being antithetic. Crustal thickness = 35 km, $T_e = 10$ km, and initial fault dip = 60° . (a) Basin geometry and crustal structure at syn-rift stage. (b) End syn-rift removal of footwall uplift by erosion, which has induced further flexural-isostatic rebound. (c) Present day post-rift geometry and crustal structure. The modelled basin depth is comparable with that observed. (d) Comparison of basin depth predicted by the flexural cantilever model (solid lines) with observed basin depth (* ornament). Vertical exaggeration = 4.

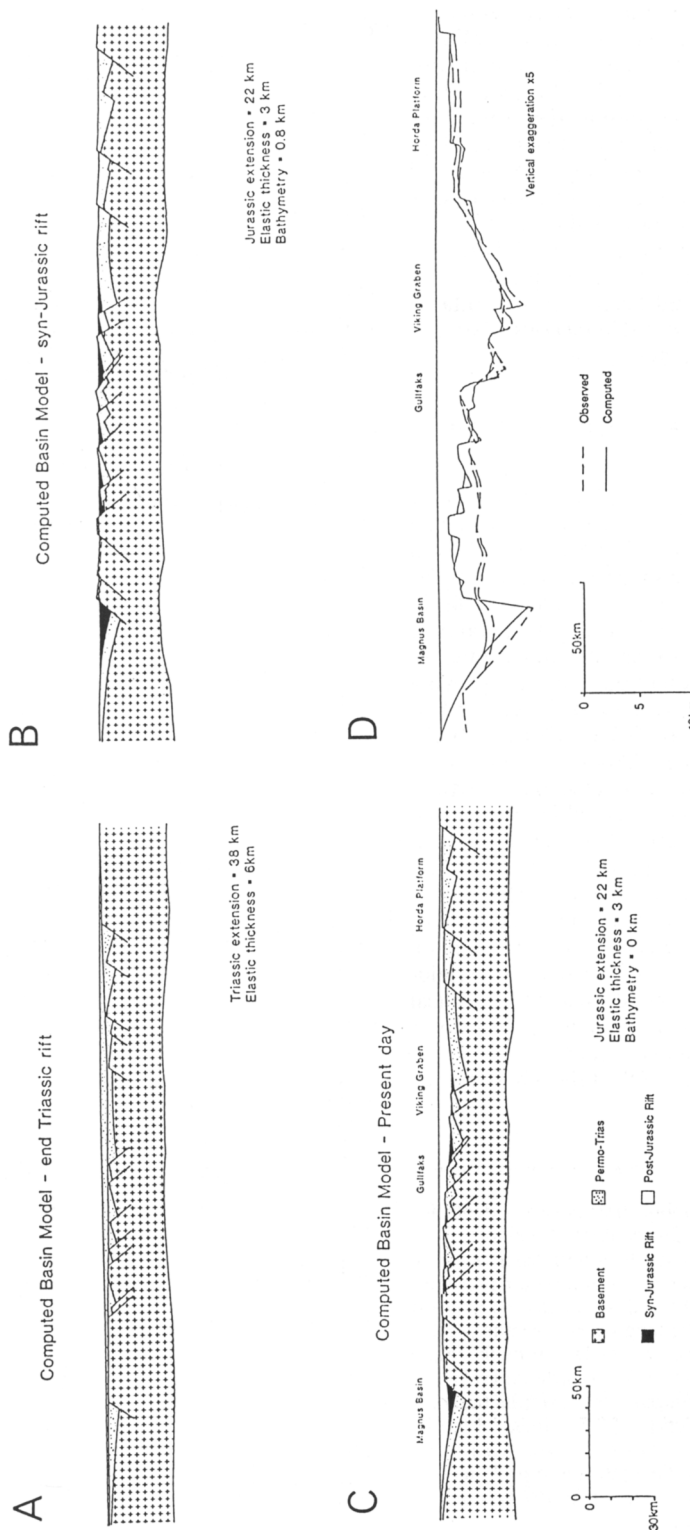


Fig. 14. Application the flexural cantilever model to a northern North Sea profile, running across the Viking Graben from the Magnus Basin (NW) to the Horda Platform (SE) (from Marsden *et al.* 1990). Predicted crustal structure and basin geometry: (a) at the end of the Middle Jurassic after initial Triassic rifting; (b) at the end of the Jurassic after Late Jurassic rifting; (c) at the present day after Cretaceous – Tertiary post-rift thermal subsidence. (d) comparison of modelled and observed thicknesses of Jurassic syn-rift and Cretaceous-Tertiary post-rift basin fill. Vertical exaggeration = 4.

quences predicted by the flexural cantilever model are shown at the end of the Middle Jurassic after Triassic rifting and thermal subsidence (Fig. 14a), at the end of Jurassic rifting (Fig. 14b), and at the present day after Cretaceous and Tertiary thermal subsidence (Fig. 14c). A comparison of observed and modelled Jurassic syn-rift and Cretaceous–Tertiary post-rift thicknesses are shown in Figure 14d. The agreement is generally good. The model predicts the uplift and erosion of the rotated fault block crests over the Shetland Terrace (e.g. Gullfaks) and the large thickness of Cretaceous–Tertiary within the Viking Graben.

Bending stresses and the effective elastic thickness

A best fit of observed and calculated basin geometry for the Viking Graben is achieved using an effective elastic thickness (T_e) of 6 km for the initial Triassic extension and 3 km for the subsequent Jurassic rifting. The best fit T_e for the Jeanne d'Arc basin is slightly greater at 10 km. Application of the flexural cantilever model to the formation of the Lake Tanganyika rift in East Africa (Kusznir & Morley 1990) gives a value of T_e of 3 km. Flexural back-stripping of the same Viking Graben profile described above gives a Cretaceous–Tertiary T_e of 3 km or less (Kusznir, unpublished results).

These values of T_e are substantially less than the 15–20 km or so thickness of the brittle seismogenic layer which contains the planar faults. The T_e is by definition the thickness of an unbroken, perfectly elastic lithosphere plate that would have the same effective flexural rigidity as the lithosphere. What then is the physical relationship between the T_e and the thickness of the brittle seismogenic layer?

The flexural bending of the lithosphere associ-

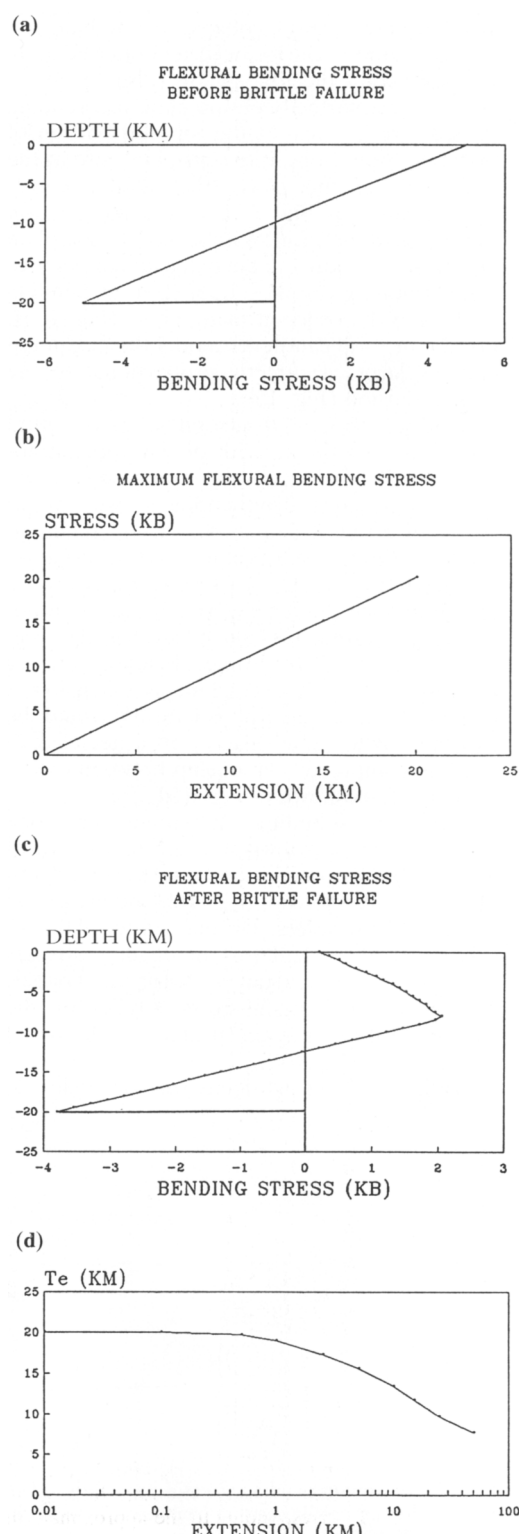


Fig. 15. (a) Elastic bending stresses versus depth for a perfectly elastic plate 20 km thick. Maximum bending stress = \pm 5 kbars. (b) Relationship between maximum elastic bending stress and fault extension predicted by the flexural cantilever model. Fault dip = 60° . T_e = 20 km. (c) Bending stresses versus depth after brittle failure within a plate 20 km thick. Initial elastic bending stress = \pm 5 kb. Brittle failure envelopes have been computed by Griffiths theory using a coefficient of friction of 0.5, a uniaxial tensile strength of 0.2 kbars and an overburden density of 3.0 g cm^{-3} . (d) The predicted decrease in T_e with increase in fault extension, due to brittle failure generated by bending stresses.

ated with the flexural ‘collapse’ of the hanging-wall and uplift of the footwall generates bending stresses within the lithosphere (also see Buck 1988). For a perfectly elastic plate the bending stresses are greatest at the top and bottom of the plate (but of opposite sign), and zero at the mid-depth of the plate (the neutral fibre), as illustrated in Fig. 15a. Using the flexural cantilever model, for an unbroken elastic plate of thickness 20 km, 7.5 km extension on a single planar fault, gives maximum flexural bending stresses of the order of many kilobars (Fig. 16a). For the flexural cantilever model the maximum bending stress is directly proportional to the fault extension (Fig. 15b).

Bending stresses of several kilobars would exceed the brittle strength of the upper lithosphere and cause extensive fracturing of the brittle upper crust. The bending stresses would still be distributed over a thickness of 20 km but would be limited to lie within the brittle-failure envelope (Fig. 15c). This brittle failure would greatly reduce the flexural rigidity of the lithosphere generating a T_c much less than the original value of 20 km. Since bending stresses increase with fault extension, as extension is increased the degree of fracturing would be expected to increase, leading to a decrease in T_c . The computed relationship between extension and T_c is shown in Fig. 15d.

The corresponding maximum bending stresses to those shown in Fig. 16a, for T_c of 3 km (still distributing the stresses over a depth of 20 km) are shown in Fig. 16b and are of the order of 1 kbar or less. The mathematical theory relating to the calculation of bending stresses will be described in detail in a subsequent paper. The maximum-bending-stress profile for the Jurassic Viking graben profile is shown in Fig. 17.

While the values of effective elastic thickness,

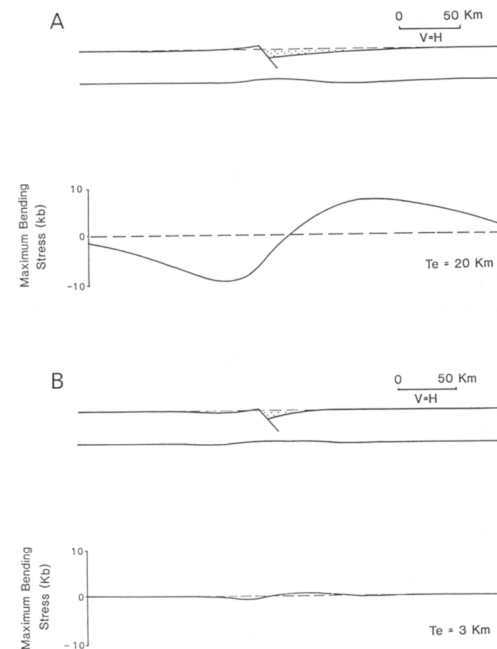


Fig. 16. Maximum bending stresses predicted by the flexural cantilever model arising from 7.5 km extension on a planar fault initially dipping at 60°. (a) No brittle failure. $T_c = 20$ km with flexural bending stresses distributed over 20 km depth. (b) With brittle failure. $T_c = 3$ km with flexural bending stresses distributed over 20 km depth, corresponding to the brittle-elastic upper crust.

T_c , operative during continental rifting may be small and of the order of only a few kilometres, it should be noted that the difference between $T_c = 0$ and $T_c = 3$ km, for example, is substantial in terms of the geological consequences. For small but finite values of T_c , of the

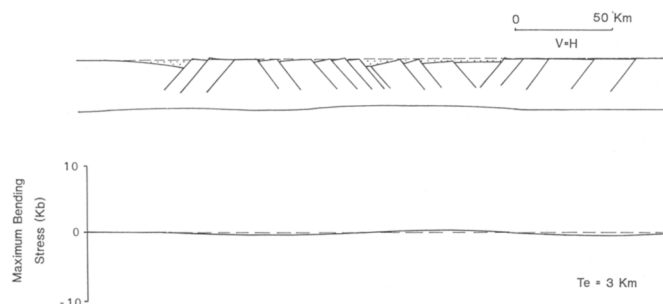


Fig. 17. Maximum bending stresses, after brittle failure, predicted by the flexural cantilever model for the Viking Graben profile, arising from Late Jurassic rifting. $T_c = 3$ km. Bending stresses are distributed over a depth of 20 km corresponding to the approximate thickness of the brittle scismogenic layer.

order of a few kilometres, footwall uplift and the familiar ‘domino-style’ block rotations of extensional tectonics can occur. However if the elastic thickness T_c were zero, corresponding to perfect Airy isostasy, these processes would not occur and their associated structural and sedimentological consequences would be absent.

We are indebted to our colleagues within the Department of Earth Sciences at the University of Liverpool and elsewhere for their valuable inspiration, discussion, help and encouragement. In particular we would like to thank (in alphabetical order!): Mike Badley, Derek Blundell, Garry Karner, Mark Newall, Alan Roberts, Tony Tankard, John Walsh, Juan Watterson, Rob Westaway, Graham Yielding and Peter Ziegler. Dave Barr and Joe Cartwright provided very useful critical reviews of this paper.

Appendix A: a description of the flexural cantilever model

1. The flexural cantilever model assumes that continental lithosphere extension occurs by planar faulting in the upper crust and plastic deformation in the lower crust and mantle (Fig. A1).

2. Let us first consider the effects of the extension of the upper crust by the planar fault. Consider a hypothetical lithosphere in which there is no mantle, only crust, and as a consequence no Moho with its associated density contrast (Fig. A2a). The planar fault is assumed to terminate at some depth within a fluid of similar density to the upper crust. If the planar fault is given a horizontal displacement E and the footwall and hangingwall blocks are kept in contact, in the absence of gravity, the geometry shown in Fig. A2b results. The upper crustal surface $u(x)$ is given by

$$\begin{aligned} u(x) &= 0 & x < 0 \\ u(x) &= x \tan(\theta) & 0 < x < E \\ u(x) &= E \tan(\theta) & E < x \end{aligned}$$

where $x = 0$ corresponds to the horizontal coordinate of the footwall cutoff and θ is the dip of the planar fault.

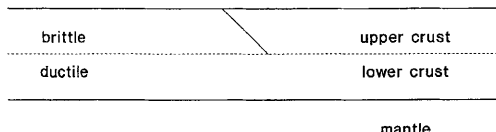


Fig. A1. Lithosphere extension is assumed to take place by planar faulting in the brittle upper crust and distributed (pure-shear) deformation within the lower crust and mantle.

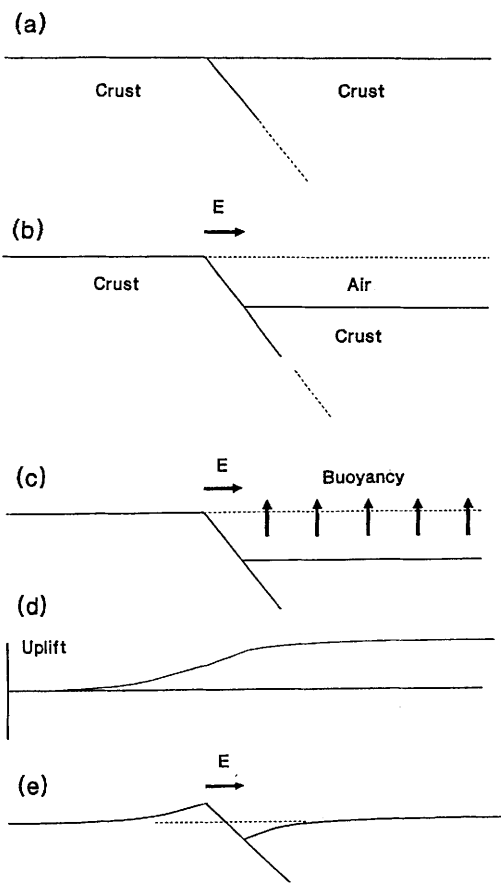


Fig. A2. Diagram summarizing the flexural isostatic interaction of foot-and hangingwall blocks during extension on a planar fault, neglecting the density contrast across the Moho between crust and mantle. See text for further explanation.

For the geometry shown in Fig. A2b, crust has been replaced by air in the hangingwall region. If gravity is ‘switched on’ this will result in a buoyancy force acting in the hangingwall (Fig. A2c). The buoyancy force, $I_b(x)$ is given by

$$I_b(x) = -u(x) \rho_c g$$

where ρ_c is crustal density and g is gravitational acceleration.

Assuming that this buoyancy force is distributed flexurally, i.e. the lithosphere has finite flexural strength, then the flexural-isostatic uplift shown in Fig. A2d results. The flexural-isostatic uplift $w_b(x)$ can be computed in the wavenumber domain by

$$W_b(k) = R(k) L_b(x)$$

where $R(k)$ is the isostatic response function such that

$$R(k) = 1/((\rho_c - \rho_a) g + Dk^4)$$

and D is flexural rigidity, k is wavenumber = $2\pi/\lambda$, and ρ_a is the density of air. $W_b(k)$ and $L_b(k)$ are the Fourier transforms of $w_b(x)$ and $l_b(x)$ respectively.

If this uplift is applied to the post-extensional geometry shown in Fig. A2b, then the foot- and hangingwall geometry shown in Fig. A2e results. The resultant upper crustal surface $s(x)$ is given by

$$s(x) = u(x) + w_b(x).$$

3. Let us consider the conservation of brittle upper crust, thickness t , during the extension process (Fig. A3a). During the extension process an area $E t$ of upper brittle crust is laterally taken out of the section. Four regions are identified in Fig. A3a (areas A, B, C and D). By conservation of area

$$E t + A - B - C + D = 0$$

where a gain in area is positive and a loss negative. Since $A = B$ this becomes

$$E t - C + D = 0.$$

Clearly the upper crustal layer around the fault loses an area equivalent to $(C - D)$ at its base. This loss of area at the base of the brittle upper crust will be compensated by an upward flow of the fluid lower crust. This inward flow of the fluid lower crust will in turn be compensated by an upward flow of fluid mantle material. The resultant perturbation of the Moho assuming vertical flow is shown in Fig. A3b and results in abrupt Moho topography. It is perhaps more reasonable to assume that the ductile flow within the lower crust and mantle, arising from area conservation, would become more distributed with increasing depth as shown in Fig. A3c. Whatever the geometry of the flow, an area $(C - D)$ of lower crust will be replaced by mantle. No density contrast is yet assumed to exist across the Moho between crust and mantle.

4. The ductile lower crust is also assumed to be thinned by pure-shear during extension. A fundamental assumption of the coupled simple-shear/pure-shear model is that extension in the upper lithosphere on planar faults is balanced at depth by pure-shear extension.

Let us assume that the pure-shear beneath the brittle-ductile transition is localized and can be represented by a sinusoidal pure-shear stretching factor (cf. McKenzie 1978) β such that

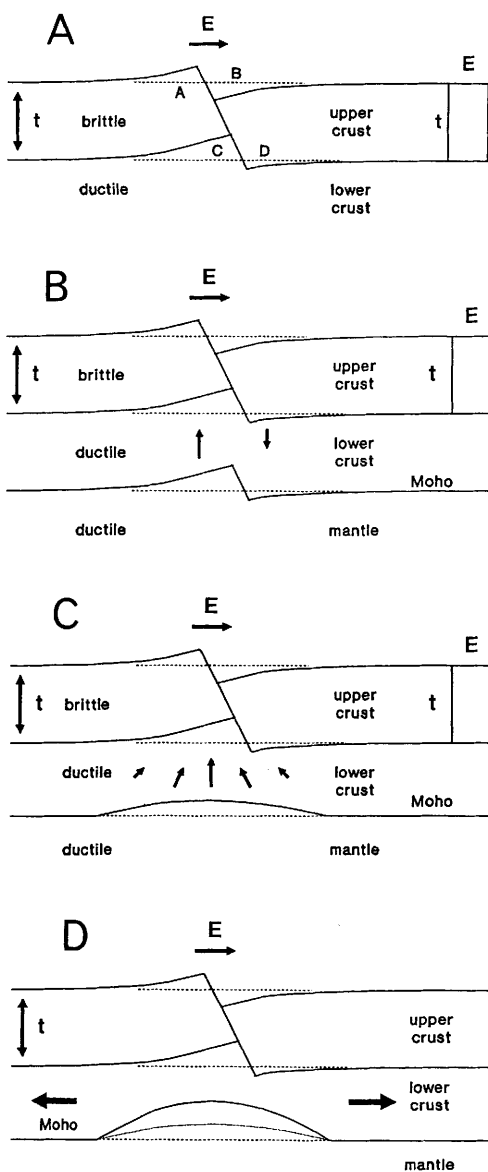


Fig. A3. Diagram summarizing mass conservation requirements following brittle, upper-crustal extension and the associated ductile flow in the lower crust and mantle and consequent perturbation of the Moho. See text for further explanation.

$$\beta = 1 + C \sin (\pi x/W)$$

where $1 + C$ is the maximum stretching β factor (N.B. $\beta = 1$ represents no extension), and W is the width of the pure-shear region.

Upper lithosphere extension E by faulting (simple-shear) must be exactly balanced by deep lithosphere extension by pure-shear.

Hence

$$E = \int_0^{W'} (\beta(x) - 1) dx \\ = \int_0^{W'} C \sin(\pi x/W) dx$$

where W' is the pre-extension width of the pure-shear region.

Provided $W \gg E$ integration of the above equation yields

$$E = 2C W'/\pi$$

or

$$C = (\pi E)/(2(W - E))$$

where W is post-extension pure-shear width.

5. The thinning of the lower crust by pure-shear extension will also cause an elevation of the Moho. If $r_{lc}(x)$ is this Moho elevation due to lower crustal pure-shear

$$r_{lc}(x) = -(d - t)(1 - 1/\beta_{lc}(x))$$

where d is crustal thickness, $\beta_{lc}(x)$ is the stretching factor in the lower crust and mantle, and depth is measured positive down.

The elevation of the Moho due to the thinning of the upper brittle crust, $r_{uc}(x)$, may also be represented by a pure-shear stretching factor $\beta_{uc}(x)$ such that

$$r_{uc}(x) = -t(1 - 1/\beta_{uc}(x)).$$

The total elevation of the Moho, $r(x)$ due to 'real' pure-shear in the lower crust and 'pseudo' pure-shear in the upper crust is given by

$$r(x) = -(d - t)(1 - 1/\beta_{lc}(x)) \\ - t(1 - 1/\beta_{uc}(x)).$$

If the 'real' and 'pseudo' pure-shear are given the same shape such that $\beta_{lc}(x) = \beta_{uc}(x) = \beta(x)$ then

$$r(x) = -(d - t)(1 - 1/\beta(x)) - t(1 - 1/\beta(x)) \\ = -d(1 - 1/\beta(x)).$$

The resultant upward perturbation of the Moho is represented in Fig. A3d.

6. Any vertical displacement which disturbs the Moho will invoke an isostatic restoring force by virtue of the density contrast between crust and mantle. If the Moho is elevated by $r(x)$, a load $l_m(x)$ will be generated such that

$$l_m(x) = r(x)(\rho_c - \rho_m)g$$

where ρ_m is mantle density.

The flexural-isostatic response $w_m(x)$ arising from this load is given by

$$W_m(k) = R(k)L_m(k)$$

$$\text{where } R(k) = 1/((\rho_m - \rho_a)g + Dk^4).$$

7. The resultant surface topography, Moho and fault geometries are given by

Surface topography

$$s(x) = u(x) + w_b(x) + w_m(x)$$

Moho topography

$$m(x) = d + r(x) + w_m(x)$$

Fault geometry

$$f(x) = x \tan(\theta) + w_b(x) + w_m(x).$$

8. Other isostatic loads are generated during both syn- and post-rift stages of basin formation and must be included in the model. These are as follows.

Syn-rift

Thermal uplift (computed using pure-shear approximation); sediment fill (computed iteratively); erosion (computed iteratively).

Post-rift

Thermal subsidence (computed using pure-shear approximation); sediment fill (computed iteratively); compaction.

Flexure for all loads is calculated in the wave-number domain using

$$W(k) = R(k)L(k).$$

References

- BARR, D. 1987. Lithospheric stretching, detached normal faulting and footwall uplift. In: COWARD, M. P., DEWEY, J. F. & HANCOCK, P. L. (eds). *Continental Extensional Tectonics*. Geological Society, London, Special Publication **28**, 75–94.
- BUCK, R. W. 1988. Flexural Rotation of Normal Faults. *Tectonics*, **7**, 959–973.
- GIBBS, A. D. 1984. Structural evolution of extensional basin margins. *Journal of the Geological Society, London*, **141**, 609–620.
- HUBBARD, R. J. 1988. Age and significance of Sequence Boundaries on Jurassic and Early Cretaceous Rifted Continental Margin. *American Association of Petroleum Geologists Bulletin*, **72**, 49–72.
- HEISKANEN, W. A. & VENING-MEINESZ, F. A. 1958. *The Earth and its gravity field*. McGraw-Hill, New York.
- JACKSON, J. A. 1987. Active normal faulting and crustal extension. In: COWARD, M. P., DEWEY, J. F. & HANCOCK, P. L. (eds). *Continental Exten-*

- sional Tectonics. Geological Society, London, Special Publication **28**, 3–17.
- & MCKENZIE, D. P. 1983. The geometrical evolution of normal fault systems. *Journal of Structural Geology*, **5**, 471–482.
- KEEN, C. E., BOUTILIER, R., DE VOOGD, B., MUDFORD, B. & ENACHESCU, M. E. 1987. Crustal geometry and extensional models for the Grand Banks, eastern Canada: constraints from deep seismic reflection data. In: BEAUMONT, C. & TANKARD, A. J. (eds). *Sedimentary basins and basin forming mechanisms*. Canadian Society of Petroleum Geologists, Memoir **12**, 101–115.
- KING, G. C. P., STEIN, R. S. & RUNDLE, J. B. 1988. The Growth of Geological Structures by Repeated Earthquakes, 1, Conceptual Framework. *Journal of Geophysical Research*, **93**, 13307–19.
- KUSZNIR, N. J. & EGAN, S. S. 1990. Simple-shear and Pure-shear models of extensional sedimentary basin formation: application to the Jeanne d'Arc Basin, Grand Banks of Newfoundland. In: TANKARD, A. J. & BALKWILL, H. R. (eds) *Extensional Tectonics of the North Atlantic Margins*. American Association of Petroleum Geologists Memoir **46**, 305–322.
- & KARNER, G. D. 1985. Dependence of the flexural rigidity of the continental lithosphere on rheology and temperature. *Nature*, **316**, 138–142.
- & MATTHEWS, D. H. 1988. Deep seismic reflections and the deformational mechanisms of the continental lithosphere. *Journal of Petrology*, Special Lithosphere Issue, 66–87.
- & MORLEY, C. 1990. The Lake Tanganyika Rift, East Africa: Application of the Flexural Cantilever Model of Continental Extension. *Geophysical Journal International*, **101**, 275.
- & PARK, R. G. 1984. Intrapllate lithosphere deformation and the strength of the lithosphere. *Geophysical Journal of the Royal Astronomical Society*, **70**, 513–538.
- & — 1987. The extensional strength of the continental lithosphere: its dependence on geothermal gradient, crustal composition and thickness. In: COWARD, M. P., DEWEY, J. F. & HANCOCK, P. L. (eds). *Continental Extensional Tectonics*. Geological Society, London, Special Publication **28**, 35–52.
- MARSDEN, G., YIELDING, G., ROBERTS, A. M. & KUSZNIR, N. J. 1990. Application of a flexural cantilever simple-shear/pure-shear model of continental lithosphere to the formation of the northern North Sea Basin. In: BLUNDELL, D. J. & GIBBS, A. D. (eds). *Tectonic Evolution of the North Sea Rifts*, Oxford University Press, 236–257.
- MCKENZIE, D. 1978. Some remarks on the development of sedimentary basins. *Earth and Planetary Science Letters*, **40**, 25–32.
- ROBERTS, A. M. & YIELDING, G. (This volume). Deformation around basin-margin faults in the North Sea/mid-Norway Rift.
- STEIN, R. S. & BARRENTOS, S. E. 1985. Planar High-Angle Faulting in the Basin and Range: Geodetic Analysis of the 1983 Borah Peak, Idaho, Earthquake. *Journal of Geophysical Research*, **90**, 11355–66.
- , KING, G. C. P. & RUNDLE, J. B. 1988. The Growth of Geological Structures by Repeated Earthquakes, 2, Field Examples of Continental Dip-Slip Faults. *Journal of Geophysical Research*, **93**, 13319–31.
- TANKARD, A. J., WELSINK, H. J. & JENKINS, W. A. M. 1990. Structure and stratigraphy of the Jeanne D'Arc Basin offshore Newfoundland: Analysis of Basin Subsidence, In: TANKARD, A. J. & BALKWILL, H. R. (eds) *Extensional Tectonics of the North Atlantic Margins*. American Association of Petroleum Geologists Memoir **46**.
- VERRALL, P. 1981. *Structural Interpretation with Applications to North Sea Problems*. Joint Association for Petroleum Exploration Courses Course Notes No. 3.
- WALSH, J. J. & WATTERSON, J. 1987. Distribution of cumulative displacement and seismic slip on a single normal fault surface. *Journal of Structural Geology*, **9**, 1039–1046.
- WEISSEL, J. K. & KARNER, G. D. 1989. Flexural uplift of rift flanks due to mechanical unloading of the lithosphere during extension. *Journal of Geophysical Research*, **94**, 13919–50.
- WERNICKE, B. 1985. Uniform-sense normal simple-shear of the continental lithosphere. *Canadian Journal of Earth Sciences*, **22**, 108–125.